Modified Couple Stress Theory for Vibration of Embedded Bioliquid-Filled Microtubules under Walking a Motor Protein Including Surface Effects

A. Ghorbanpour Arani [1, 2] [*], M. Abdollahian [1], A.H. Ghorbanpour-Arani [1]

[1]*Faculty of Mechanical Engineering, University of Kashan, Kashan , Islamic Republic of Iran*
[2]*Institute of Nanoscience & Nanotechnology, University of Kashan, Kashan, Islamic Republic of Iran*

ABSTRACT

Microtubules (MTs) are fibrous and tube-like cell substructures exist in cytoplasm of cells which play a vital role in many cellular processes. Surface effects on the vibration of bioliquid MTs surrounded by cytoplasm is investigated in this study. The emphasis is placed on the effect of the motor protein motion on the MTs. The MT is modeled as an orthotropic beam and the surrounded cytoplasm is assumed as an elastic media which is simulated by Pasternak foundation. In order to consider the small scale effects, the modified couple stress theory (MCST) is taken into account. An analytical method is employed to solve the motion equations obtained by energy method and Hamilton's principle. The influence of surface layers, bioliquid, surrounding elastic medium, motor proteins motion, and small scale parameter are shown graphically. Results demonstrate that the speed of motor proteins is an effective parameter on the vibration characteristics of MTs. It is interesting that increasing the motor proteins speed does not change the maximum and minimum values of MTs dynamic deflection. The presented results might be useful in biomedical and biomechanical principles and applications.

© 2015 IAU, Arak Branch.All rights reserved.

Keywords : Dynamic deflection; Motor protein movement; Bioliquid-filled microtubules; Cytoplasm; Modified couple stress theory.

1 INTRODUCTION

EUKARYOTIC cytoskeleton which supplies the configuration and structure of the cells, are composed of three main types of cytoskeleton filaments: actin filaments, intermediate filaments and MTs. Among these filaments, MTs are stronger than the other filaments. Therefore, MTs are more responsible for the cell rigidity. MTs have vital roles in many cellular processes, as an example of forming the mitotic spindle, guiding and facilitating intracellular motions of organelles, and support kinesins to convert chemical energy into mechanical work. As shown in Fig. 1, MTs consist of strings of αβ-tubulin heterodimers, so-called protofilaments, which are arranged in parallel forming a hollow cylinder whose length ranges from 10 nm to 100 μm.

---

[*] Corresponding author. Tel.: +98 31 55912450; Fax: +98 31 55912424.
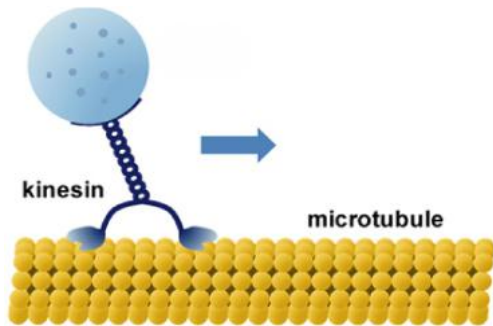*E-mail address: aghorban@kashanu.ac.ir* (A. Ghorbanpour Arani).

Fig.1
MTs under walking a kinesin.

MTs almost function in concert with the molecular motors that move on them. These motor proteins attach to different consignment, including organelles and vesicles, and pull them along the surface of the microtubule. These applications make MTs as one of the most components of each cell and investigation of mechanical behaviors of such structures becomes one of the appealing topics in biomechanics. Wang and Zhang [1] used an orthotropic shell model to investigate in detail the long axial wavelength circumferential vibration of MTs. Cifra et al. [2] investigated the electric field generated by axial vibration modes of MTs. Fundamental frequency analysis of MTs under different boundary conditions using differential quadrature method was investigated by Mallakzadeh et al. [3]. Li et al. [4] quantitatively showed that as modeled as an elastic beam, the flexural rigidity of MTs depend on their length, as a result of strongly anisotropic elastic properties of MTs. Mechano-electrical vibrations of MTs-link to subcellular morphology was investigated by Kucera and Havelka [5].

In order to study the mechanical characteristics of nano and microstructures, the small scale effects should be taken into account. Therefore, applying higher order continuum in mechanical modeling of such structures is necessary. Among these theories nonlocal elasticity theory attracted many investigators. For instance, buckling and postbuckling analysis was presented by Shen [6] for MTs subjected to torsion in thermal environments. He showed that the small scale effect plays an important role in the postbuckling of MTs. A continuum model based on the nonlocal elasticity theory was developed by Gao and Lei [7] for MTs that were considered as a Timoshenko beam. Demir and Civalek [8] investigated the torsional and axial free vibration analyses of MTs. They obtained governing equations of motions based on the nonlocal elasticity theory for both continuous and discrete modeling. In another study, Civalek and Akgoz [9] applied the nonlocal elasticity theory to MTs for the first time. They presented free vibration analysis of MTs based on Euler-Bernoulli (EBB) model. However, some authors employed the other theories such as strain gradient theory (SGT) and modified couple stress theory (MCST). The classical couple stress theory considers two material length scale parameters besides the classical constants for an isotropic elastic material. After some modifications by researchers, the MCST was expressed. In the MCST one additional material length scale parameter is considered in addition to the classical material constants and the couple stress tensor is assumed to be symmetric. Based on the modified strain gradient theory, and by using the linear and nonlinear EBB models vibration of protein MTs was investigated by Karimi Zeverdejani and Tadi Beni [10]. The consistent governing equations for the buckling for MTs were derived by Akgoz and Civalek [11] using SGT. They discussed the influence of the length scale parameter on the buckling characteristics of MTs. Based on MCST, a new Timoshenko beam model was established to address the size effect of MTs by Fu and Zhang [12].

In order to investigate the mechanical characteristics of MTs, one cannot neglect the effect of the cytoplasm. As the cytoplasm is a gel like substance, it can be modeled as Winkler type elastic medium. But, for more accuracy one can model the cytoplasm as Pasternak foundation which considers both normal pressure and transverse shear stress caused by interaction of shear deformation of the elastic medium. Gao and An [13] studied the buckling behaviors of MTs in a living cell based on the nonlocal anisotropic shell theory and Stokes flow theory. A nonlocal shear deformable shell model was developed for buckling of MTs embedded in an elastic matrix cytoplasm by Shen [14]. In another attempt he [15] presented the large amplitude flexural vibration behavior for MTs embedded in an elastic matrix of cytoplasm. Also Taj and Zhang [16, 17] developed an orthotropic Pasternak model to investigate vibration and wave propagation of embedded MTs.

Recently, it has become clear that when materials and structures shrink to micrometers, surface effects often play a critical role in their static or dynamical behavior due to increasing ratio of surface/inter face area to volume. Only a few researchers consider the effect of surface layers on the mechanical behaviors of MTs. For instance, a new explicit formula was presented by Farajpour et al. [18] for the length-dependent persistence length of MTs with consideration of surface layer.

Investigating the influence of the bioliquid on the mechanical characteristics of MTs is so new that only a couple of papers have considered the effect of bioliquid in MTs. In this regard, Wang et al. [19] presented an analytical solution for the coupling influence of initial stress, surface layers and scale-dependent on the frequency characteristics of bioliquid-filled MTs. Also, the results of an investigation into the coupling vibration of bioliquid-filled MTs embedded in bio-medium reported by Li et al. [20].

Apart the mentioned papers and due to the best of author's knowledge, one can strongly say that there is not any work on the mechanical behaviors of microtubules under walking of motor proteins. In order to generate the force to carry out the work of pulling or contracting, motor proteins convert chemical energy to mechanical energy. There are three families of motor proteins: kinesins, dyneins and myosins. Among these, kinesins and dyneins walking along the MTs. Motivated by these considerations, in this study kinesins and dyneins motions modeled as a microparticle moving along the MT and the surface effects on the vibration characteristics of bioliquid-filled MTs is investigated based on an orthotropic EBB model. Further, the MCST is employed to consider the small scale effects and also, the surrounded cytoplasm is simulated as Pasternak elastic foundation.

2 GOVERNING MOTION EQUATION

2.1 Preliminaries

Figs. 2 depicts a bioliquid-filled MT under a walking motor protein with length L, inner radius R_i, outer radius R_o, mean radius R and the thickness h, embedded in cytoplasm with surface layers. Also, x_k is the position of the motor protein such as kinesin and v_k denotes the kinesin speed.

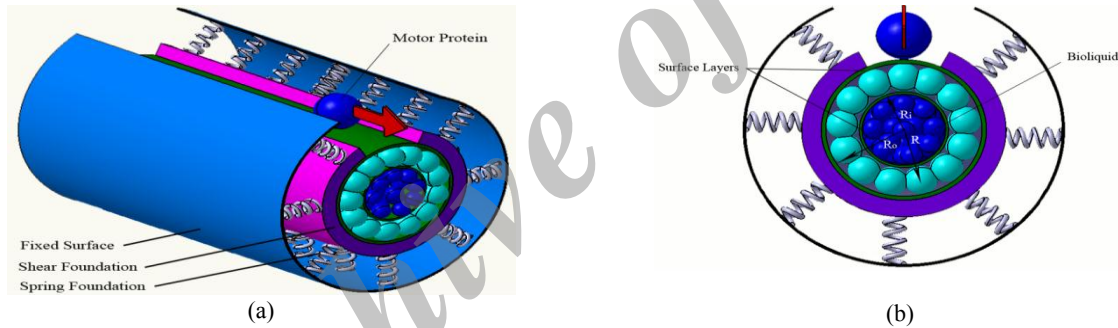(a)   (b)

Fig.2
Bioliquid-filled microtubules under a walking motor protein with surface layers.

The MT is modeled as an orthotropic EBB model and therefore the displacement field based on EBB theory becomes [9]:

$$u_1(x,z,t) = u(x,t) - z\frac{\partial w(x,t)}{\partial x},$$ (1a)

$$u_2(x,z,t) = 0,$$ (1b)

$$u_3(x,z,t) = w(x,t),$$ (1c)

where u_1, u_2 and u_3 represent the total displacement of the MT in x, y and z directions, respectively. Also, u and w are the middle surface displacements. Therefore, the only nonzero component of strain tensor based on EBB model will be obtained as:

$$\varepsilon_{xx} = \frac{\partial u}{\partial x} - z\frac{\partial^2 w}{\partial x^2}.$$ (2)

2.2 Strain energy

Based on the MCST the strain energy density U of an elastic body occupying volume V can be written as [21-24]:

$$U = \frac{1}{2}\int_V \left(\sigma_{ij}\varepsilon_{ji} + m_{ij}\chi_{ij} \right)dV + \frac{1}{2}\left(\int_{S^+} \sigma_{ij}^s \varepsilon_{ij}^s dS^+ + \int_{S^-} \sigma_{ij}^s \varepsilon_{ij}^s dS^- \right)(i,j = 1,2,3),$$

(3)

where σ_{ij} is the Cauchy stress tensor, ε_{ij} is the strain tensor, m_{ij} is the deviatoric part of the couple stress tensor, χ_{ij} is the symmetric curvature tensor, the upper index S is related to the surface layers, in which for orthotropic materials [25, 26]:

$$\varepsilon_{ij} = \frac{1}{2}\left(u_{i,j} + u_{j,i} \right),$$

(4a)

$$\chi_{ij} = \frac{1}{2}\left(\theta_{i,j} + \theta_{j,i} \right),$$

(4b)

$$\begin{Bmatrix} \sigma_{xx} \\ \sigma_{yy} \\ \sigma_{zz} \\ \sigma_{xz} \\ \sigma_{yz} \\ \sigma_{xy} \end{Bmatrix} = \begin{bmatrix} Q_{11} & Q_{12} & Q_{13} & 0 & 0 & 0 \\ Q_{21} & Q_{22} & Q_{23} & 0 & 0 & 0 \\ Q_{31} & Q_{32} & Q_{33} & 0 & 0 & 0 \\ 0 & 0 & 0 & Q_{44} & 0 & 0 \\ 0 & 0 & 0 & 0 & Q_{55} & 0 \\ 0 & 0 & 0 & 0 & 0 & Q_{66} \end{bmatrix} \begin{Bmatrix} \varepsilon_{xx} \\ \varepsilon_{\theta\theta} \\ \varepsilon_{zz} \\ 2\varepsilon_{xz} \\ 2\varepsilon_{yz} \\ 2\varepsilon_{xy} \end{Bmatrix},$$

(4c)

$$\begin{Bmatrix} m_x \\ m_y \\ m_{xy} \\ m_{yx} \end{Bmatrix} = \begin{bmatrix} 2lQ_{55} & 0 & 0 & 0 \\ 0 & 2lQ_{44} & 0 & 0 \\ 0 & 0 & Q_{44}l^2 & Q_{55}l^2 \\ 0 & 0 & Q_{44}l^2 & Q_{55}l^2 \end{bmatrix} \begin{Bmatrix} \chi_x \\ \chi_y \\ \chi_{xy} \\ \chi_{yx} \end{Bmatrix},$$

(4d)

where θ_i are the components of the rotation vector, δ_{ij} is the Kronecker delta, l is the material length scale parameter. It can be concluded from Eq. (3) that considering the size effects yields higher strain energy values and therefore higher frequencies. It should be mentioned that nonlocal elasticity theory predicts lower frequency values than that those predicted by classical theory.

The constitutive equations for surface layers can be written as [27]:

$$\sigma_{\alpha\beta}^s = \tau_s \delta_{\alpha\beta} + \left(\tau_s + \lambda_s \right)\varepsilon_{\gamma\gamma}\delta_{\alpha\beta} + 2\left(\mu_s - \tau_s \right)\varepsilon_{\alpha\beta} + \tau_s u_{\alpha,\beta}^s,$$

(5a)

$$\sigma_{\alpha z}^s = \tau_s u_{z,\alpha}^s, \left(\alpha,\beta = x,y \right),$$

(5b)

where λ_s and μ_s denote the Lame parameters of surface layers and τ_s is the residual surface stress under unconstrained conditions. Using Eqs. (5) yields the following surface stresses as:

$$\sigma_{xx}^s = \left(\lambda_s + 2\mu_s \right)\varepsilon_{xx} - \frac{\tau_s}{2}\left(\frac{\partial w}{\partial x} \right)^2 + \tau_s,$$

(6a)

$$\sigma_{xz}^s = \tau_s \frac{\partial w}{\partial x}.$$

(6b)

Based on the Gurtin-Murdoch model unlike classical plate theories, σ_{zz} is not equal to zero on the inner and outer surfaces. Indeed, the stress component σ_{zz} varies linearly along the MT thickness and satisfies the balance condition on the surfaces which can be expressed as the following relation:

$$\sigma_{zz} = \frac{1}{2}\left(\sigma_z^+ + \sigma_z^-\right) + \frac{z}{h}\left(\sigma_z^+ - \sigma_z^-\right)$$
$$= \frac{1}{2}\left(\frac{\partial \sigma_{xz}^s}{\partial x} - \rho_s \frac{\partial^2 w}{\partial t^2}\right)^+ + \frac{1}{2}\left(\frac{\partial \sigma_{xz}^s}{\partial x} - \rho_s \frac{\partial^2 w}{\partial t^2}\right)^- + \frac{z}{h}\left(\frac{\partial \sigma_{xz}^s}{\partial x} - \rho_s \frac{\partial^2 w}{\partial t^2}\right)^+ - \frac{z}{h}\left(\frac{\partial \sigma_{xz}^s}{\partial x} - \rho_s \frac{\partial^2 w}{\partial t^2}\right)^-. \tag{7}$$

Using Eqs. (7) yields:

$$\sigma_{zz} = \frac{2z}{h}\left(\tau_s \frac{\partial^2 w}{\partial x^2} - \rho_s \frac{\partial^2 w}{\partial t^2}\right), \tag{8}$$

In which ρ_s is the mass density of surface layers. Applying the σ_{zz} obtained in Eq. (8) and using Eqs. (2) and (4) the only nonzero component of stress tensor can be obtained as follows:

$$\sigma_{xx} = C_{11}\left[\frac{\partial u}{\partial x} - z \frac{\partial^2 w}{\partial x^2}\right] + v\sigma_{zz}, \tag{9}$$

where $C_{11} = Q_{11} - \frac{Q_{13}^2}{Q_{33}}$ and $v = \frac{Q_{13}}{Q_{33}} = \frac{v_x(1+v_\theta)}{1-v_x v_\theta}$. Also, the stiffness constants Q_{ij} are presented in Appendix A. Also, the components of rotation vector can be expressed in terms of the components of the displacement as:

$$\theta_i = \frac{1}{2}e_{ijk}u_{k,j}, \tag{10}$$

In which e_{ijk} is the permutation symbol. Hence, the only nonzero rotation vector components can be obtained by using Eqs. (1) into Eq. (10) as:

$$\theta_y = -\frac{\partial w}{\partial x}. \tag{11}$$

Substituting Eq. (11) into Eq. (4b), it can be obtained:

$$\chi_{xy} = \frac{1}{2}\left(-\frac{\partial^2 w}{\partial x^2}\right). \tag{12}$$

The strain energy of the MT can be obtained by using Eqs. (2) and (12) into Eq. (3) as:

$$U = \frac{1}{2}\int_x\left[\bar{N}_x \frac{\partial u}{\partial x} - \bar{M}_x \frac{\partial^2 w}{\partial x^2} - \frac{P_{xy}}{2}\frac{\partial^2 w}{\partial x^2}\right]dx + \frac{1}{2}\int_x\left[N_x^s \frac{\partial u}{\partial x} - M_x^s \frac{\partial^2 w}{\partial x^2}\right]dx \tag{13}$$

where:

$$\left(\bar{N}_x, \bar{M}_x\right) = \int_A \sigma_{xx}(1,z)dA, \left(N_x^s, M_x^s\right) = \int_S \sigma_{xx}^s(1,z)dS, P_{xy} = \int_A m_{xy}dA, \tag{14}$$

The strain energy of the system expressed in Eq. (13) can be rewritten as follows:

$$U = \frac{1}{2}\int_x \left[N_x \frac{\partial u}{\partial x} - M_x \frac{\partial^2 w}{\partial x^2} - \frac{P_{xy}}{2}\frac{\partial^2 w}{\partial x^2} \right] dx \tag{15}$$

where:

$$N_x = \bar{N}_x + N_x^s, M_x = \bar{M}_x + M_x^s \tag{16}$$

Using Eqs. (6a), (8), (9) and (4d), Eqs. (16) can is obtained as follows:

$$N_x = \left(C_{11}A\right)^* \frac{\partial u}{\partial x} + \tau_s 2\pi\left(R_i + R_o\right) - \frac{\tau_s}{2}2\pi\left(R_i + R_o\right)\left(\frac{\partial w}{\partial x}\right)^2, \tag{17a}$$

$$M_x = -\left(C_{11}I\right)^* \frac{\partial^2 w}{\partial x^2} + \frac{2\nu I}{h}\left(\tau_s \frac{\partial^2 w}{\partial x^2} - \rho_s \frac{\partial^2 w}{\partial t^2}\right), \tag{17b}$$

$$P_{xy} = -Q_{44}l^2 A \frac{\partial^2 w}{\partial x^2}, \tag{17c}$$

where $A = 2\pi R h$ and $I = \pi R^3 h$ are the cross sectional area and second moment of inertia of the MT, respectively. Also:

$$\left(C_{11}A\right)^* = C_{11}A + 2\pi\left(R_i + R_o\right)\left(\lambda_s + 2\mu_s\right), \tag{18a}$$

$$\left(C_{11}I\right)^* = C_{11}I + \pi\left(R_i^3 + R_o^3\right)\left(\lambda_s + 2\mu_s\right). \tag{18b}$$

2.3 Strain energy

The kinetic energy of the MT *K* including surface effects can be written as:

$$K = \frac{1}{2}\int_0^L \int_A \left(\rho + \rho_s\right)\left[\left(\frac{\partial u_1}{\partial t}\right)^2 + \left(\frac{\partial u_2}{\partial t}\right)^2 + \left(\frac{\partial u_3}{\partial t}\right)^2\right] dA\, dx, \tag{19}$$

where ρ is the MT mass density. Substituting Eqs. (1) into Eq. (19), yields the kinetic energy of MT as:

$$\delta K = \int_0^L \left[I_0\left(\frac{\partial^2 u}{\partial t^2} + \frac{\partial^2 w}{\partial t^2}\right) + I_2 \frac{\partial^4 w}{\partial x^2 \partial t^2}\right] dx, \tag{20}$$

where:

$$I_0 = I_0^* + I_0^s = \int_A \rho\, dA + \int_A \rho_s\, dA, \tag{21a}$$

$$I_2 = I_2^* + I_2^s = \int_A \rho z^2\, dA + \int_A \rho_s z^2\, dA. \tag{21b}$$

2.4 Energy associated by external works

The energy associated with external works V including surrounding elastic medium, the bioliquid-filled p_f and the distributed transverse load along longitudinally axis p can be calculated as follows [19,20,28]:

$$V = \frac{1}{2}\int_0^L \left(-K_w w + K_g \nabla^2 w + p_f + p\right)w dx, \tag{22}$$

where K_w and K_g denote the spring constant of the Winkler type and the shear constant of the Pasternak type, respectively. Also, $\nabla^2 = \partial^2 / \partial x^2$ is the Laplace vector.

2.5 Bioliquid effect

Assuming the cylindrical coordinate system (r, θ, x), the induced force of the dynamic pressure from the bioliquid can be obtained as [19, 20]:

$$p_f = \int_0^{2\pi} -\rho_f \frac{\partial \varphi(r, \theta, x, t)}{\partial t} \cos\theta R_i d\theta, \tag{23}$$

where t, ρ_f are the time variable and the bioliquid mass density. Moreover $\varphi(r, \theta, x, t)$ is the velocity potential function which should be satisfy the Laplace equation in cylindrical coordinate system as:

$$\nabla^2 \varphi = 0 \rightarrow \frac{\partial^2 \varphi}{\partial x^2} + \frac{\partial^2 \varphi}{\partial r^2} + \frac{1}{r}\frac{\partial u}{\partial r} + \frac{1}{r^2}\frac{\partial^2 \varphi}{\partial \theta^2} = 0. \tag{24}$$

2.5.1 For MTs are closed at one end and open at another end (C-O)

For the bioliquid end conditions is assumed to be closed at $x = 0$ and opened at $x = L$. The relevant boundary conditions for the bioliquid in MT can be written as [19,20]:

$$x = 0 \xrightarrow{close\,end} \left.\frac{\partial \varphi}{\partial x}\right|_{x=0} = 0, \tag{25a}$$

$$x = L \xrightarrow{Open\,end} P_{x=L} = 0 \rightarrow \left.\frac{\partial \varphi}{\partial t}\right|_{x=L} = 0. \tag{25b}$$

The solution of Eq. (24) can be written as [19, 20]:

$$\varphi(r, \theta, x, t) = \sum_{m=1,3,5}^{\infty} \sum_{n=1,3,5}^{\infty} G_{mn}(r)\cos(n\theta)\cos\left(\frac{m\pi}{2L}x\right)\dot{T}(t), \tag{26}$$

where $T(t)$ is the unknown time-dependent generalized coordinates.

2.5.2 For MTs are closed at both ends (C-C)

The end conditions for MTs are closed at both ends can be written as follows [29]:

$$\varphi(r,\theta,x,t) = \sum_{m=1}^{\infty} \sum_{n=1,3,5}^{\infty} G_{mn}(r)\cos(n\theta)\cos\left(\frac{m\pi}{L}x\right)\dot{T}(t), \tag{27}$$

Substituting Eqs. (26) into Eq. (24) yields the following Bessel equation as:

$$G_{mn}''(r_m) + \frac{1}{r_m}G_{mn}'(r_m) - \left(1 + \frac{n^2}{r_m^2}\right)G_{mn}(r_m) = 0, \tag{28}$$

In which $r_m = (m\pi/2L)r$ for MTs are closed at one end at opened at another end and $r_m = (m\pi/L)r$ for MTs closed at both ends . The solution to the Eq. (27) can be obtained in terms of modified Bessel functions as:

$$G_{mn}(r_m) = A_{mn}I_n(r_m) + B_{mn}K_n(r_m), \tag{29}$$

where $I_n(r_m)$ and $K_n(r_m)$ are the first and second types of modified Bessel functions, respectively. The velocity potential function must have a finite value at $r = 0$, therefore, $K_n(r_m)$ should be equal to zero. Also, the first types of modified Bessel function $I_n(r_m)$ can be expressed as follows:

$$I_n(r_m) = \sum_{k=0}^{\infty} \frac{1}{k!\Gamma(k+n+1)}\left(\frac{r_m}{2}\right)^{n+2k}. \tag{30}$$

No cavitation is assumed at the fluid shell interface at $r = R_i$, therefore:

$$\left.\frac{\partial\varphi}{\partial r}\right|_{r=R_i} = \frac{\partial w}{\partial t}\cos\theta, \tag{31}$$

where w is the transverse displacement at middle surface of the simply-supported MT which can be written as:

$$w(x,t) = \sum_{n=1}^{\infty} W_n\left[\sqrt{2}\sin\left(\frac{n\pi x}{L}\right)\right]T_n(t), \tag{32}$$

where n is the number of vibration modes and W_n is the deflection amplitude due to the bending, respectively. Substituting Eqs. (26), (27) and (32) into Eq. (31), using Eq. (29), the orthotropic condition of the $\cos(m\pi x/2L)$ for C-O end conditions and $\cos(m\pi x/L)$ for C-C end conditions and comparing the coefficient of both sides the following relations can be obtained as:

$$For\ C - O\ end\ conditions \begin{cases} A_{m1} = \dfrac{2}{L}\dfrac{\displaystyle\int_0^L W(x)\cos\left(\dfrac{m\pi}{2L}x\right)dx}{\left[\dfrac{dI_1(r)}{dr}\right]_{r=R_i}}(m=1,3,5\cdots,n=1), \\ A_{mn} = 0\ (n \neq 1). \end{cases} \tag{33}$$

$$For\,C-C\,end\,conditions\begin{cases} A_{m1} = \dfrac{2}{L}\dfrac{\int_0^L W(x)\cos\left(\dfrac{m\pi}{L}x\right)dx}{\left[\dfrac{dI_1(r)}{dr}\right]_{r=R_i}}(m=1,2,3,\cdots,n=1),\\[20pt] A_{mn}=0\,(n\neq1). \end{cases}\tag{34}$$

Substituting Eqs. (33) and (34) into (29), using the obtained relation in Eq. (26) and applying the velocity potential function in the Eq. (23), the induced force from the dynamic pressure of the bioliquid in MTs for both C-O and C-C end conditions can be calculated.

2.6 Kinesin walking effect

In order to modeling the kinesin movement on the MT the following assumptions are considered [30, 31]:
- The motor protein is assumed as a microparticle.
- The velocity of the motor protein is constant.
- The initial effects of the motor protein are negligible.
- The friction force between the motor protein and MT is negligible.

The effect of motor protein motion on the MT has been considered by load $P(x,t)$ as a Dirac-delta function as follows [30, 31]:

$$P(x,t)=P\delta(x-x_k),\tag{35}$$

In which P denotes the magnitude of the moving load induced by motor protein walking, δ is the Dirac-delta function.

2.7 Motion equations

The motion equations of embedded bioliquid-filled MT can be derived using Hamilton's principle given as follows:

$$\int_0^t (\delta U-\delta K-\delta V)dt=0,\tag{36}$$

Substituting Eqs. (13), (19) and (21) into Eq. (36), motion equation in transverse direction is obtained as follows:

$$-\frac{\partial}{\partial x}\left(N_x\frac{\partial w}{\partial x}\right)-\frac{\partial^2 M_x}{\partial x^2}-\frac{\partial^2 P_{xy}}{\partial x^2}+I_0\frac{\partial^2 w}{\partial t^2}+I_2\frac{\partial^4 w}{\partial x^2 \partial t^2}+K_w w-K_g\frac{\partial^2 w}{\partial x^2}-p_f-p=0.\tag{37}$$

Finally, using Eqs. (17), (22) and (35) into Eq. (37), the governing motion equation in transverse direction for each end conditions can be expressed as:

2.7.1 Motion equations for C-O end conditions

$$\begin{aligned}&\left[(C_{11}I)^*-\frac{2\nu I}{h}\tau_s+Q_{44}Al^2\right]\frac{\partial^4 w}{\partial x^4}+\left[-2\pi\tau_s(R_i+R_o)-K_g\right]\frac{\partial^2 w}{\partial x^2}+K_w w\\[6pt]&-\left(I_2-\frac{2\nu I}{h}\rho_s\right)\frac{\partial^4 w}{\partial x^2 \partial t^2}+I_0\frac{\partial^2 w}{\partial t^2}-P\delta(x-x_k)\\[6pt]&+\sum_{m=1,3,5}^{\infty}\frac{2\pi R_i\rho_f\ddot{T}(t)}{L}\frac{I_1(R_i)}{\left.\dfrac{dI_1(r)}{dr}\right|_{r=R_i}}\cos\left(\frac{m\pi x}{2L}\right)\int_0^L\sum_{n=1}^{\infty}W_n\left[\sqrt{2}\sin\left(\frac{n\pi x}{L}\right)\right]\cos\left(\frac{m\pi x}{2L}\right)dx=0.\end{aligned}\tag{38a}$$

2.7.2 Motion equations for C-C end conditions

$$\left[\left(C_{11}I\right)^* - \frac{2\nu I}{h}\tau_s + Q_{44}Al^2\right]\frac{\partial^4 w}{\partial x^4} + \left[-2\pi\tau_s\left(R_i + R_o\right) - K_g\right]\frac{\partial^2 w}{\partial x^2} + K_w w$$

$$-\left(I_2 - \frac{2\nu I}{h}\rho_s\right)\frac{\partial^4 w}{\partial x^2 \partial t^2} + I_0\frac{\partial^2 w}{\partial t^2} - P\delta\left(x - x_k\right)$$

$$+ \sum_{m=1}^{\infty}\frac{2\pi R_i \rho_f \ddot{T}\left(t\right)}{L}\frac{I_1\left(R_i\right)}{\left.\dfrac{dI_1\left(r\right)}{dr}\right|_{r=R_i}}\cos\left(\frac{m\pi x}{L}\right)\int_0^L\sum_{n=1}^{\infty}W_n\left[\sqrt{2}\sin\left(\frac{n\pi x}{L}\right)\right]\cos\left(\frac{m\pi x}{L}\right)dx = 0. \tag{38b}$$

3   SOLUTION PROCEDURES

Substituting Eq. (32) into Eqs. (38), multiplying both sides of the resulting equations with $\sqrt{2}\sin\left(k\pi x/L\right)$, integrating them over the domain (0,L) and using the orthogonality condition yields the following equations for both end conditions as:

$$\left\{\left(\frac{n\pi}{L}\right)^4\left[\left(C_{11}I\right)^* - \frac{2\nu I}{h}\tau_s + Q_{44}Al^2\right] + \left(\frac{n\pi}{L}\right)^2\left[2\pi\tau_s\left(R_i + R_o\right) + K_g\right] + K_w\right\}T\left(t\right)$$

$$+ \left[\left(\frac{n\pi}{L}\right)^2\left(I_2 - \frac{2\nu I}{h}\rho_s\right) + I_0 + 2\pi R_i \rho_f\sum_{m=1,3,5}^{\infty}\frac{I_1\left(R_i\right)}{\left.\dfrac{dI_1\left(r\right)}{dr}\right|_{r=R_i}}F_{nm}^2\right]\ddot{T}\left(t\right) \tag{39}$$

$$- \frac{P}{L}\int_0^L\sqrt{2}\delta\left(x - x_k\right)\sin\left(\frac{n\pi x}{L}\right)dx = 0,$$

In which for C-O end conditions:

$$F_{nm} = \frac{1}{L}\int_0^L\sqrt{2}\sin\left(\frac{n\pi x}{L}\right)\cos\left(\frac{m\pi x}{2L}\right)dx. \tag{40}$$

And for C-C end conditions:

$$F_{nm} = \frac{1}{L}\int_0^L\sqrt{2}\sin\left(\frac{n\pi x}{L}\right)\cos\left(\frac{m\pi x}{L}\right)dx. \tag{41}$$

The following relation may be used for the Dirac-delta function integration:

$$\int_{x_1}^{x_2}f\left(x\right)\delta^n\left(x - x_0\right)dx = \begin{cases}\left(-1\right)^n f^n\left(x_0\right) & x_1 < x_0 < x_2 \\ 0 & otherwise\end{cases} \tag{42}$$

where δ^n denoted the nth derivative of Dirac-delta function. For both end conditions Eq. (39) can be rewritten by using Eq. (42) as:

$$\ddot{T}_n\left(t\right) + \omega_n^2 T_n\left(t\right) = \frac{\sqrt{2}P}{LM}\sin\left(\frac{n\pi x_k}{L}\right), \tag{43}$$

In which $\omega_n^2 = \dfrac{K_n}{M_n}$ and:

$$K_n = \left(\frac{n\pi}{L}\right)^4 \left[\left(C_{11}I\right)^* - \frac{2\nu I}{h}\tau_s + Q_{44}Al^2\right] + \left(\frac{n\pi}{L}\right)^2 \left[2\pi\tau_s\left(R_i + R_o\right) + K_g\right] + K_w \tag{44a}$$

$$M_n = \left(\frac{n\pi}{L}\right)^2 \left(I_2 - \frac{2\nu I}{h}\rho_s\right) + I_0 + 2\pi R_i \rho_f \sum_{m=1,3,5}^{\infty} \frac{I_1\left(R_i\right)}{\left.\dfrac{dI_1\left(r\right)}{dr}\right|_{r=R_i}} F_{nm}^2 \tag{44b}$$

Solving Eq. (40) yields:

$$T_n\left(t\right) = \frac{\sqrt{2}P}{LM}\left[\frac{\dfrac{i\,\pi\nu_k}{\omega_n L}\sin\omega_n t - \sin\left(\dfrac{i\,\pi\nu_k t}{L}\right)}{\left(\dfrac{i\,\pi\nu_k}{L}\right)^2 - \omega_n^2}\right]. \tag{45}$$

Substituting Eq. (45) into Eq. (32) yields the dynamic deflection of MT and therefore the normalized dynamic deflection can be defined as:

$$\bar{w}\left(x,t\right) = \frac{w\left(x,t\right)}{w_{st}}, \tag{46}$$

where represents the static deflection of nanotube under a point load at the mid-span and:

$$w_{st} = \frac{PL^3}{48\left(C_{11}I\right)^*}, \tag{47}$$

4   RESULTS AND DISCUSSION

Based on an analytical method and orthotropic EBB model the effect of motor protein motion on an embedded bioliquid-filled MT considering surface effects are obtained in this study. In the following figures, the effects of parameters such as material length scale parameter, velocity of motor protein, aspect ratio, elastic medium and surface layers are investigated. Mechanical and geometrical properties of the 13_3 MT are tabulated in Table 1.

Table 1
Mechanical and geometrical properties of the 13_3 MT.

Parameter	Value	References
Inner radius of MT, R_i	$8.7nm$	[15]
Outer radius of MT, R_o	$12.7nm$	[15]
Mean radius of MT, R	$10.7nm$	[15]
Length of MT, L	$100R$	[15]
Wall thickness of MT, h	$1.6nm$	[15]
Mass density per unit volume, ρ	$1.47\,g/cm^3$	[15, 19, 20]
Longitudinal Young's modulus, E_x	$1GPa$	[4, 15, 32]
Circumferential Young's modulus, E_θ	$1MPa$	[17]
Poisson's ratio in axial direction, ν_x	0.3	[4, 15, 32]
Shear modulus, Q_{44}	$10^{-5}GPa$	[15, 33]

At first, times history of normalized deflection of MT midpoint is investigated in Figs. 3(a-d)to further study the motor protein velocity for the first four modes. It is fascinating to note that MT has the positive and the negative deflections as if it vibrates under a moving harmonic load. It is seen that the variation of midpoint normalized dynamic deflection is constant for all mode as the motor protein velocity changes. Furthermore, from Figs.3(a-d), it can be observed that in the period of vibration, as the motor protein velocity increases the MT have more harmonic movement in all modes. Also, it is interesting to note that the dynamic deflection is higher in first and third modes than the second and forth modes.
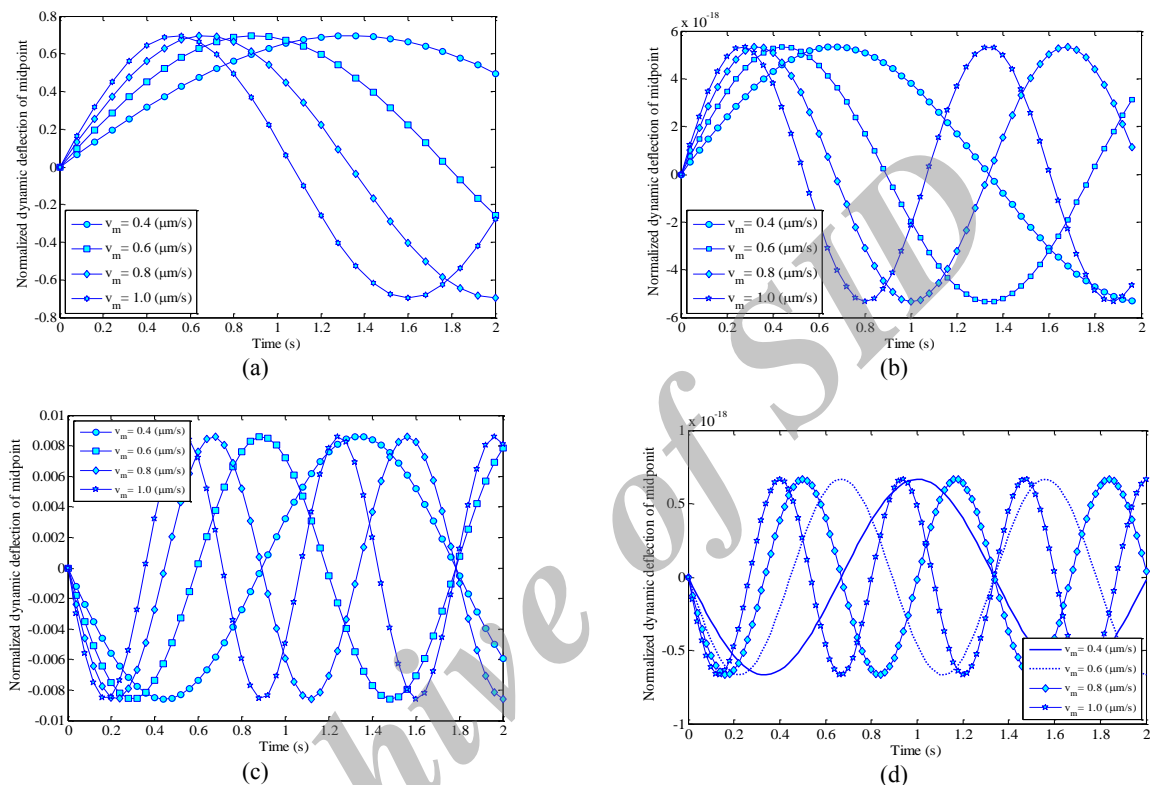
Fig.3
Time history of normalized deflection of MT midpoint for a) 1st mode b) 2nd mode c) 3rd mode d) 4th mode.

The effect of motor protein velocity on the normalized deflection of simply supported Mt each point is illustrated in Figs. 4(a-d) for first four modes at $t = 1(s)$. As can be seen from Fig. 4(a) the maximum value of normalized deflection for the first mode is located at the MT midpoint whereas, Figs. 4(b) and 4(d)shows that for the second and fourth modes the minimum deflection take places at the midpoint.

Fig. 5 depicts the midpoint normalized deflection at $t = 1(s)$ versus the motor protein velocity for different values of aspect ratio. Obviously, the maximum and minimum values of normalized deflection remain constant by increasing the motor protein velocity. Though, as the velocity of motor protein increases, for lower aspect ratio values the normalized deflection of MT oscillates more between its minimum and maximum values.

Fig. 6 presents the influence of material length scale parameter on the normalized dynamic deflection of MT versus the dimensionless distance along the length. As can be observed the dynamic deflection is decreased with increasing the material length scale parameter. It is due to the fact that material length scale parameter makes the MT perform stiffer. The obtained results are coinciding with those obtained by Reddy et al. [21]. This result can be obtained from mathematical point of view, too. It is seen from Eq. (41) that the dynamic deflection is inversely proportional to the material length scale parameter.

Fig. 7 demonstrates the plots of normalized dynamic deflection of the MT across the dimensionless distance along the length for different surface elastic constants with $\rho_s = 0 \left(Kg/m^3 \right)$, $\tau_s = 0.9108 \left(N/m \right)$ and $t = 1(s)$. It is seen that increasing the surface elastic constants from negative to positive values decreases the normalized

dynamic deflection. It is due to the fact that increasing the surface elasticity, increases the bending stiffness of MT. The obtained results are in accordance with those obtained by Ansari et al. [34].
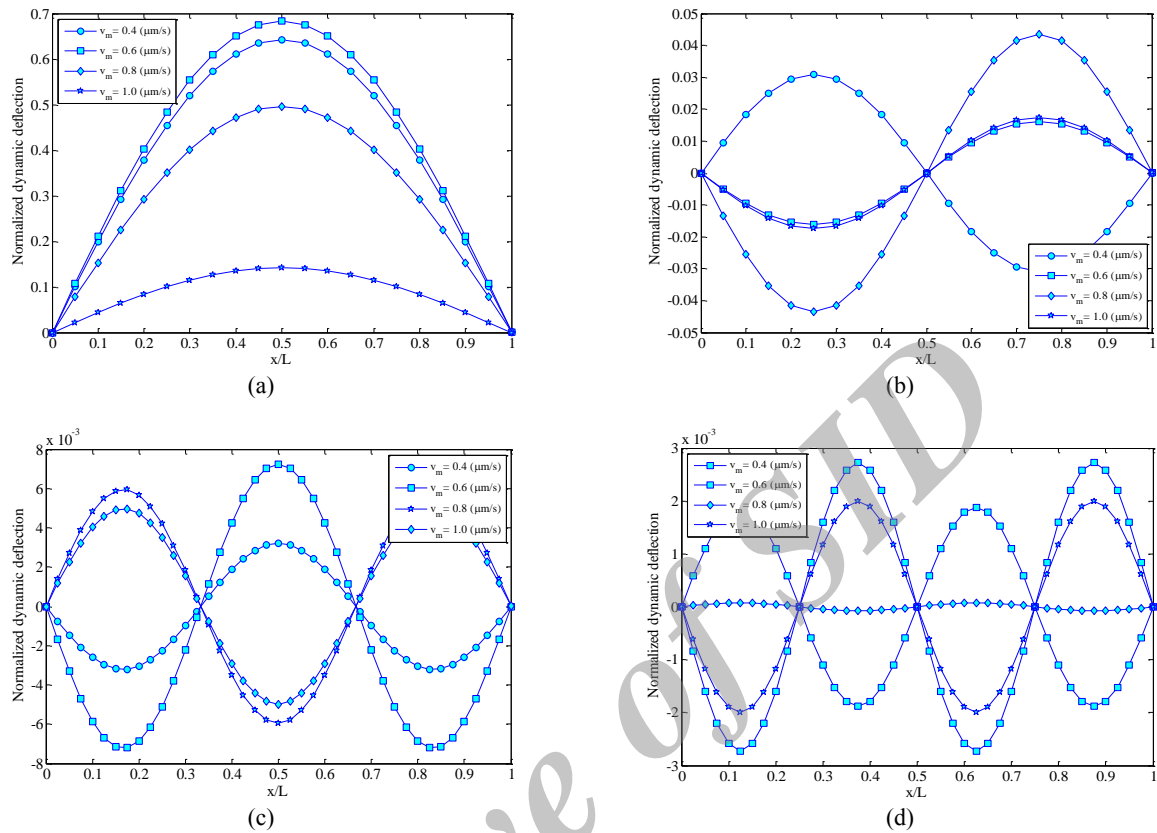
Fig.4
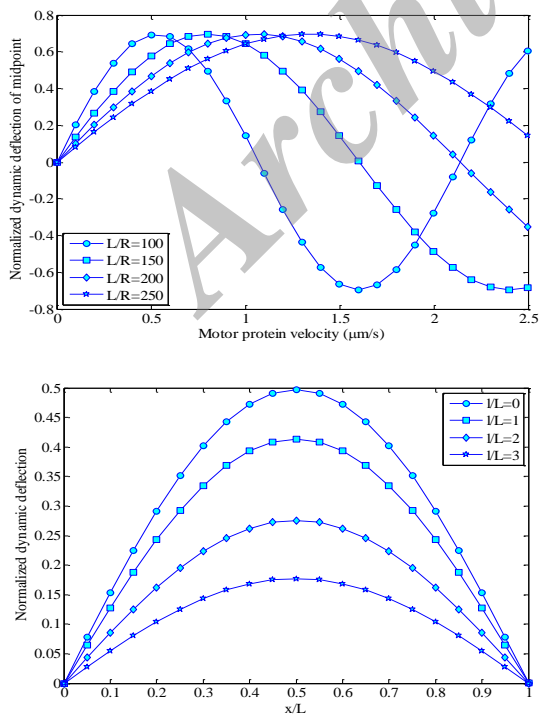Normalized deflection versus dimensionless distance along the length a) 1st mode b) 2nd mode c) 3rd mode d) 4th mode.

Fig.5
Normalized deflection of MT midpoint versus motor protein velocity for different aspect ratio values.

Fig.6
Influence of material length scale parameter on the normalized dynamic deflection.
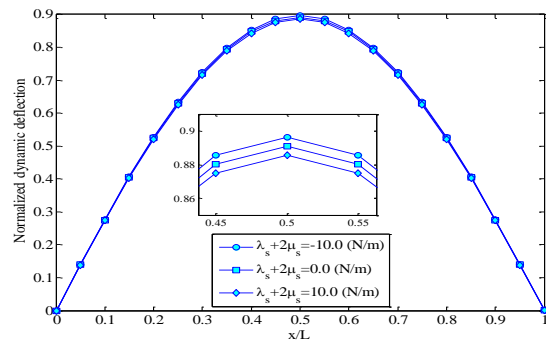
Fig.7
Effect of surface elastic constant on the normalized dynamic deflection.

Effect of surface residual stress on the normalized dynamic deflection of the MT with assuming $E_s = 5.1882(N/m), \nu_s = 0.3, \rho_s = 0(Kg/m^3)$ and $t = 1(s)$ is presented in Fig. 8. It can be conclude that the normalized dynamic deflection is reduced as the surface residual stress increases. Increasing the surface residual stresses makes the MT stiffer and therefore the dynamic deflection decreases.

Variation of frequency with respect to the surface density for different values of fluid density is illustrated in Fig. 9. It is concluded that increasing the surface density decreases the frequency of the MT. Also, variations of frequency with respect to the surface density become more prominent at lower fluid density values. Moreover, increasing the density of the fluid, reduce the frequency of the MT. therefore, one can say that increasing surface and fluid densities reduce the stability of the MT. it is also interesting to note that the deference between the frequency values is much higher at the lower surface density values as compared to higher surface density values.

In order to explore the effects of surrounding elastic medium, Fig. 10 has been plotted. As can be expected, without elastic medium the stiffness of the MT is the least and therefore the normalized deflection is the most. Appending springs and developing the Winkler foundation makes the system stiffer, and then the normalized deflection decreases. Also, similar to the Winkler foundation, increasing the shear constant of the Pasternak type, reduces the normalized deflection. Further, the effect of shear constant of the Pasternak type is more visible at lower spring constant of the Winkler type.
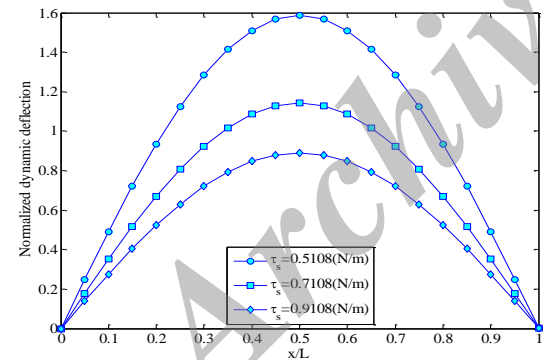

Fig.8
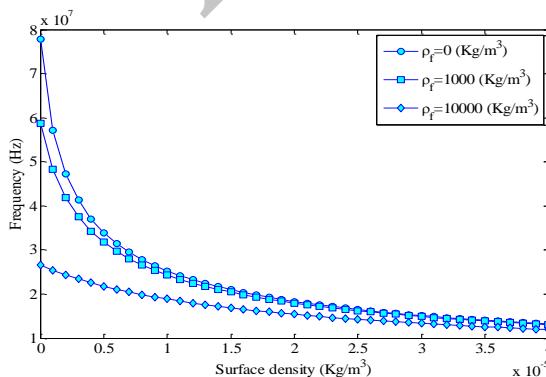Effect of surface residual stress on the normalized dynamic deflection.

Fig.9
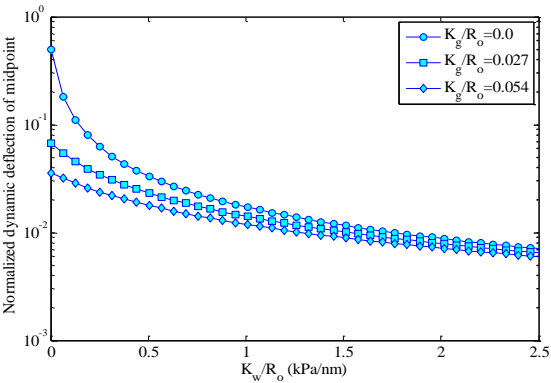Frequency with respect to the surface density for various fluid density values.

Fig.10
Influence of the elastic medium on the normalized dynamic deflection.

Fig. 11 indicates the frequency of bioliquid-filled MTs versus the material length scale parameter for different values of aspect ratio. It is seen from Fig. 11 that increasing the material length scale parameter increases the frequency of bioliquid-filled MT. therefore, it can be concluded that the results predicted based on the modified couple stress theory are larger than those predicted by the classical theory. This is due to the fact that by considering size effects in Eq. (3) the energy of the system increases, therefore, the system becomes stiffer and the frequency of the system increases. Moreover, the frequency is decreased as the aspect ratio of MT is increased.

The influences of surrounded elastic medium on the frequency of the MT are depicted in Fig. 12 for both C-C and C-O end conditions. . It is observed from Fig. 12 that increasing the Winkler and Pasternak constants increases the frequency of the system. It is due to the fact that enhancing the elastic medium parameters makes the system stiffer and therefore the frequency of the system increases. Also, it is seen that the frequency obtained for C-C end conditions are higher than those obtained by C-O end conditions.

Fig. 13 shows the effects of aspect ratio on the frequency of the MT. As can be seen the frequency is decreased with increasing the aspect ratio of the MT. Moreover, the effects of aspect ratio values become more prominent at lower Winkler constants.
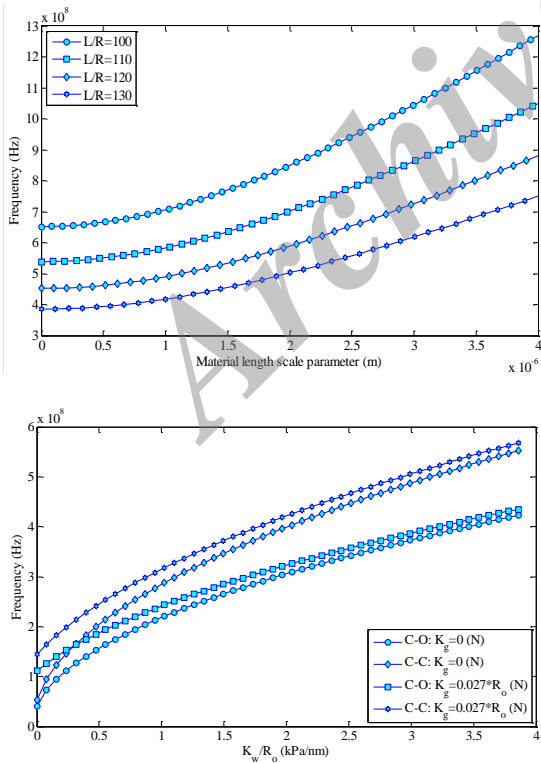

Fig.11
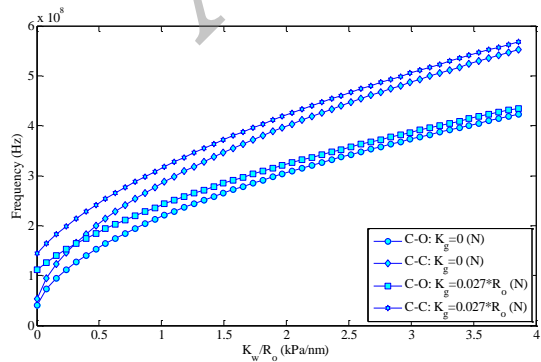Frequency versus material length scale parameter for different aspect ratio values.

Fig.12
Influences of the surrounded elastic medium on the frequency for different end conditions.
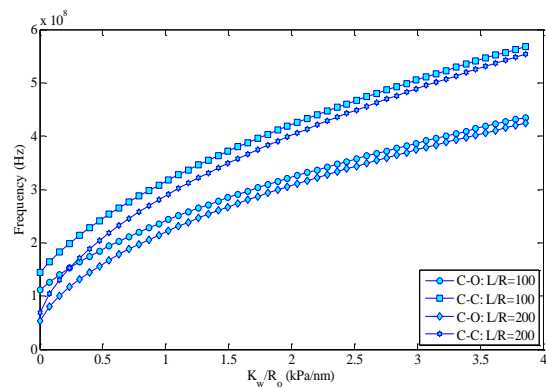
Fig.13
Frequency versus Winkler medium constant for different end conditions.

Effects of mass density of bioliquid are presented on Table 2. for both C-C and C-O end conditions. As can be seen, the effects of the mass density of the bioliquid become more visible for C-O end conditions. Additionally, the influences of end conditions will be effective at higher mass density of bioliquid values. it is also seen that increasing the mass density of bioliquid decreases the frequency and therefore the stability of the bioliquid-filled MTs.

Table 2
Effects of bioliquid mass density on the frequency of the MTs for both C-O and C-C end conditions.

End conditions	Mass Density of bioliquid										
	0	100	200	300	400	500	600	700	800	900	1000
C-O	4.2697	4.1177	3.9808	3.8567	3.7435	3.6397	3.5441	3.4557	3.3736	3.2971	3.2255
C-C	4.2697	4.2640	4.2583	4.2525	4.2469	4.2412	4.2356	4.2300	4.2244	4.2188	4.2132

Table 3. is presented so as to validate the accuracy of this study with those available in the literature. For this propose, a simplified case of the analysis is compared with the results presented by Xiang and Liew [9] and Karimi Zeverdejani and Tadi Beni [10] ignoring the surface effects, bioliquid and size effects. For this propose the material properties are assumed to be: $E_x = 2GPa$, $E_\theta = E_z = 0$, $\nu_x = 0.3$ and $\nu_\theta = \nu_z = 0$. Also the mean radius is $R = 12.8nm$. These comparisons are shown in Table 1 in which a very good agreement can be found.

Table 3
Comparison of the frequency (MHz) values of the present work with those obtained by other literature for an isolated simply supported MT.

	Theory	Length of the MTs (micrometer)			
		4	6	8	10
Xiang and Liew [9]	Atomistic continuum	-	-	-	1.01
Karimi Zeverdejani and Tadi Beni [10]	CT	6.9	3	1.7	1.02
Present work	CT	6.51	2.89	1.63	1.04

5 CONCLUSIONS

In this study, based on walking motor proteins on the MT, vibration behavior of bioliquid-filled microtubules was studied including surface effects. The surrounding cytoplasm medium was modeled as Pasternak foundation. Based on orthotropic EBB model and employing energy method and Hamilton's principle the motion equation for a bioliquid-filled MT under a walking motor protein was derived. The MCST was utilized to consider the small scale effects. Using an analytical method the frequency and dynamic deflection of the MT under a walking motor protein were obtained. Numerical results indicate that increasing both fluid and surface density decreases the frequency of MT. Further, the effect of fluid density on the normalized dynamic deflection becomes more remarkable with decreasing surface density. It is also found that increasing the material length scale parameter decreases the normalized dynamic deflection. Regarding elastic medium effect, it can be concluded that increasing both Pasternak and Winkler constants decreases the normalized dynamic deflection. In addition, increasing surface elastic constants and surface residual stress, reduces the normalized dynamic deflection. Moreover, in the period of vibration, as the

motor protein velocity increases the MT have more harmonic movement in all modes. The results of this study were validated as far as possible by Xiang and Liew [9] and Karimi Zeverdejani and Tadi Beni [10]. The results presented in this work can be useful in biomedical and biomechanical applications.

ACKNOWLEDGEMENTS

APPENDICES

In this study orthotropic EBB model is applied. For this proposed the elastic constants in Eqs. (4c) and (4d) are obtained. Consider the following compliance matrix for an orthotropic material as:

$$
S_{ij} = \begin{bmatrix}
\dfrac{1}{E_1} & -\dfrac{\nu_{21}}{E_2} & -\dfrac{\nu_{31}}{E_3} & 0 & 0 & 0 \\[2mm]
-\dfrac{\nu_{12}}{E_1} & \dfrac{1}{E_2} & -\dfrac{\nu_{32}}{E_3} & 0 & 0 & 0 \\[2mm]
-\dfrac{\nu_{13}}{E_1} & -\dfrac{\nu_{23}}{E_2} & \dfrac{1}{E_3} & 0 & 0 & 0 \\[2mm]
. & . & . & \dfrac{1}{\mu_{31}} & 0 & 0 \\[2mm]
. & . & . & . & \dfrac{1}{\mu_{23}} & 0 \\[2mm]
. & . & . & . & . & \dfrac{1}{\mu_{12}}
\end{bmatrix}
\tag{A.1}
$$

In which $\nu_{ij}/E_i = \nu_{ji}/E_j$. Eq. (A.1) can be rewritten in cylindrical coordinate system as:

$$
S_{ij} = \begin{bmatrix}
\dfrac{1}{E_x} & -\dfrac{\nu_\theta}{E_\theta} & -\dfrac{\nu_z}{E_z} & 0 & 0 & 0 \\[2mm]
-\dfrac{\nu_x}{E_x} & \dfrac{1}{E_\theta} & -\dfrac{\nu_z}{E_z} & 0 & 0 & 0 \\[2mm]
-\dfrac{\nu_x}{E_x} & -\dfrac{\nu_\theta}{E_\theta} & \dfrac{1}{E_z} & 0 & 0 & 0 \\[2mm]
. & . & . & \dfrac{1}{\mu_{31}} & 0 & 0 \\[2mm]
. & . & . & . & \dfrac{1}{\mu_{23}} & 0 \\[2mm]
. & . & . & . & . & \dfrac{1}{\mu_{12}}
\end{bmatrix}
\tag{A.2}
$$

Therefore, the following elastic constant can be obtained:

$$Q_{11} = \frac{E_x\left(1-\nu_\theta\nu_z\right)}{1-\nu_x\nu_\theta-\nu_x\nu_z-\nu_\theta\nu_z-2\nu_x\nu_\theta\nu_z}, Q_{12} = \frac{\nu_\theta E_x\left(1+\nu_z\right)}{1-\nu_x\nu_\theta-\nu_x\nu_z-\nu_\theta\nu_z-2\nu_x\nu_\theta\nu_z}, Q_{12} = \frac{\nu_z E_x\left(1+\nu_\theta\right)}{1-\nu_x\nu_\theta-\nu_x\nu_z-\nu_\theta\nu_z-2\nu_x\nu_\theta\nu_z}$$

$$Q_{21} = \frac{\nu_x E_\theta\left(1+\nu_z\right)}{1-\nu_x\nu_\theta-\nu_x\nu_z-\nu_\theta\nu_z-2\nu_x\nu_\theta\nu_z}, Q_{22} = \frac{E_\theta\left(1-\nu_x\nu_z\right)}{1-\nu_x\nu_\theta-\nu_x\nu_z-\nu_\theta\nu_z-2\nu_x\nu_\theta\nu_z}, Q_{23} = \frac{\nu_z E_\theta\left(1+\nu_x\right)}{1-\nu_x\nu_\theta-\nu_x\nu_z-\nu_\theta\nu_z-2\nu_x\nu_\theta\nu_z} \quad \text{(A.3)}$$

$$Q_{31} = \frac{\nu_x E_z\left(1+\nu_\theta\right)}{1-\nu_x\nu_\theta-\nu_x\nu_z-\nu_\theta\nu_z-2\nu_x\nu_\theta\nu_z}, Q_{12} = \frac{\nu_\theta E_z\left(1+\nu_x\right)}{1-\nu_x\nu_\theta-\nu_x\nu_z-\nu_\theta\nu_z-2\nu_x\nu_\theta\nu_z}, Q_{12} = \frac{E_z\left(1-\nu_x\nu_\theta\right)}{1-\nu_x\nu_\theta-\nu_x\nu_z-\nu_\theta\nu_z-2\nu_x\nu_\theta\nu_z}$$

REFERENCES

[1]   Wang C.Y., Zhang L.C., 2008, Circumferential vibration of microtubules with long axial wavelength, *Journal of Theoretical Biology* **41**: 1892-1896.

[2]   Cifra M., Pokorny J., Havelka D., Kucera O., 2010, Electric field generated by axial longitudinal vibration modes of microtubule, *Biosystems* **100**: 122-131.

[3]   Mallakzadeh M., Pasha Zanoosi A.A., Alibeigloo A., 2013, Fundamental frequency analysis of microtubules under different boundary conditions using differential quadrature method, *Communication in Nonlinear Science and Numerical Simulation* **18**: 2240-2251.

[4]   Li C., Ru C.Q., Mioduchowski A., 2006, Length-dependence of flexural rigidity as a result of anisotropic elastic properties of microtubules, *Biochemical and Biophysical Research Communication* **349**: 1145-1150.

[5]   Kucera O., Havelka D., 2012, Mechano-electrical vibrations of microtubules-Link to subcellular morphology, *Biosystems* **109**: 346-355.

[6]   Shen H.S., 2013, Nonlocal shear deformable shell model for torsional buckling and postbuckling of microtubules in thermal environments, *Mechanics Research Communications* **54**: 83-95.

[7]   Gao Y., Lei F.M., 2009, Small scale effects on the mechanical behaviors of protein microtubules based on the nonlocal elasticity theory, *Biochemical and Biophysical Research Communication* **387**: 467-471.

[8]   Demir C., Civalek O., 2013, Torsional and longitudinal frequency and wave response of microtubules based on the nonlocal continuum and nonlocal discrete models, *Applied Mathematical Modelling* **37**: 9355-9367.

[9]   Xiang P., Liew K.M., 2012, Free vibration analysis of microtubules based on an atomistic-continuum model, *Journal of Sound and Vibration* **331**: 213-230.

[10]   Karimi Zeverdejani M., Tadi Beni Y., 2013, The nano scale vibration of protein microtubules based on modified strain gradient theory, *Current Applied Physics* **13**: 1566-1576.

[11]   Akgoz B., Civalek O., 2011, Application of strain gradient elasticity theory for buckling analysis of protein microtubules, *Current Applied Physics* **11**: 1133-1138.

[12]   Fu Y., Zhang J., 2010, Modeling and analysis of microtubules based on a modified couple stress theory, *Physica E* **42**: 1741-1745

[13]   Gao Y., An L., 2010, A nonlocal elastic anisotropic shell model for microtubule buckling behaviors in cytoplasm, *Physica E* **42**: 2406-2415.

[14]   Shen H.S., 2010, Nonlocal shear deformable shell model for bending buckling of microtubules embedded in an elastic medium, *Physics Letter A* **374**: 4030-4039.

[15]   Shen H.S., 2011, Nonlinear vibration of microtubules in living cells, *Current Applied Physics* **11**: 812-821.

[16]   Taj M., Zhang J.Q., 2012, Analysis of vibrational behaviors of microtubules embedded within elastic medium by Pasternak model, *Biochemical and Biophysical Research Communications* **424**: 89-93.

[17]   Taj M., Zhang J.Q., 2014, Analysis of wave propagation in orthotropic microtubules embedded within elastic medium by Pasternak model, *Journal of the Mechanical Behavior Biomedical Materials* **30**: 300-305.

[18]   Farajpour A., Rastgoo A., Mohammadi M., 2014, Surface effects on the mechanical characteristics of microtubule networks in living cells, *Mechanics Research Communications* **57**: 18-26.

[19]   Wang X., Yang W.D., Xiong J.T., 2014, Coupling effects of initial stress and scale characteristics on the dynamic behavior of bioliquid-filled microtubules immersed in cytosol, *Physica E* **56**: 342-347.

[20]   Li H.B., Xiong J.T., Wang X., 2013, The coupling frequency of bioliquid-filled microtubules considering small scale effects, *European Journal of Mechanics-A/Solids* **39**: 11-16.

[21]   Reddy J.N., 2011, Microstructure-dependent couple stress theories of functionally graded beams, *Journal of the Mechanics and Physics of Solids* **59**: 2382-2399

[22]   Ansari R., Mohammadi V., Faghih Shojaei M., Gholami R., Sahmani S., 2013, Postbuckling characteristics of nanobeams based on the surface elasticity theory, *Composites Part B: Engineering* **55**: 240-246.

[23]   Shaat M., Mahmoudi F.F., Gao X.L., Faheem A.F., 2014, Size-dependent bending analysis of Kirchhoff nano-plates based on a modified couple-stress theory including surface effects, *International Journal of Mechanical Sciences* **79**: 31-37.

[24]   Shaat M., Mohamed S.A., 2014, Nonlinear-electrostatic analysis of micro-actuated beams based on couple stress and surface elasticity theories, *International Journal of Mechanical Sciences* **84** :208-217.

[25]   Mohammad Abadi M., Daneshmehr A.R., 2014, An investigation of modified couple stress theory in buckling analysis of micro composite laminated Euler–Bernoulli and Timoshenko beams, *International Journal of Engineering Sciences* **75**: 40-53.

[26]   Daneshmand F., Ghavanloo E., Amabili M., 2011, Wave propagation in protein microtubules modeled as orthotropic elastic shells including transverse shear deformations, *Journal of Biomechanics* **44**: 1960-1966.

[27]   Ansari R., Mohammadi V., Faghih Shojaei M., Gholami R., Rouhi H., 2014, Nonlinear vibration analysis of Timoshenko nanobeams based on surface stress elasticity theory, *European Journal of Mechanics-A/Solids* **45**: 143-152.

[28]   Abdollahian M., Ghorbanpour Arani A., Mosallaei Barzoki A., Kolahchi R., Loghman A., 2013, Non-local wave propagation in embedded armchair TWBNNTs conveying viscous fluid using DQM, *Physica B* **418**: 1-15.

[29]   Amabili M., 2008, *Nonlinear Vibrations and Stability of Shells and Plates*, Cambridge University Press.

[30]   Ghorbanpour Arani A., Roudbari M.A., Amir S., 2012, Nonlocal vibration of SWBNNT embedded in bundle of CNTs under a moving nanoparticle, *Physica B* **407**:3646-3653.

[31]   Simsek M., 2011, Nonlocal effects in the forced vibration of an elastically connected double-carbon nanotube system under a moving nanoparticle, *Computational Materials Science* **50**: 2112-2123.

[32]   Tuszynski J.A., Luchko T., Portet S., Dixon J.M., 2005, Anisotropic elastic properties of microtubules, *The European Physical Journal E* **17**: 29-35.

[33]   Heireche H., Tounsi A., Benhassaini H., Benzair A., Bendahmane M., Missouri M.,Mokadem S., 2010, Nonlocal elasticity effect on vibration characteristics of protein microtubules, *Physica E* **42**: 2375-2379.

[34]   Ansari R., Hosseini K., Darvizeh A., Daneshian B., 2013, A sixth-order compact finite difference method for non-classical vibration analysis of nanobeams including surface stress effects, *Applied Mathematics and Computation* **219**: 4977-4991.